九州大学学術情報リポジトリ
Kyushu University Institutional Repository

Trisaccharide containing α2,3-linked sialic acid is a receptor for mumps virus

久保田, 万理恵

https://doi.org/10.15017/1806873

出版情報：九州大学, 2016, 博士（医学）, 課程博士
バージョン：
権利関係：全文ファイル公表済

KYUSHU UNIVERSITY

Trisaccharide containing α2,3-linked sialic acid is a receptor for mumps virus

Marie Kubota[a], Kaoru Takeuchi[b,1], Shumpei Watanabe[a], Shinji Ohno[a], Rei Matsuoka[c], Daisuke Kohda[c], Shin-ichi Nakakita[d], Hiroaki Hiramatsu[e], Yasuo Suzuki[e], Tetsuo Nakayama[f], Tohru Terada[g], Kentaro Shimizu[g], Nobutaka Shimizu[h], Mitsunori Shiroishi[i], Yusuke Yanagi[a], and Takao Hashiguchi[a,1]

[a]Department of Virology, Faculty of Medicine, Kyushu University, Fukuoka 812-8582, Japan; [b]Laboratory of Environmental Microbiology, Faculty of Medicine, University of Tsukuba, Tsukuba 305-8575, Japan; [c]Division of Structural Biology, Medical Institute of Bioregulation, Kyushu University, Fukuoka 812-8582, Japan; [d]Department of Functional Glycomics, Life Science Research Center, Kagawa University, Kagawa 761-0793, Japan; [e]Health Science Hills, College of Life and Health Sciences, Chubu University, Kasugai 487-8501, Japan; [f]Laboratory of Viral Infection, Kitasato Institute for Life Sciences, Tokyo 108-8641, Japan; [g]Department of Biotechnology and Agricultural Bioinformatics Research Unit, Graduate School of Agricultural and Life Sciences, The University of Tokyo, Tokyo 113-8657, Japan; [h]Photon Factory, Institute of Materials Structure Science, High-Energy Accelerator Research Organization, Tsukuba 305-0801, Japan; and [i]Graduate School of Pharmaceutical Sciences, Kyushu University, Fukuoka 812-8582, Japan

Edited by Michael B. A. Oldstone, The Scripps Research Institute, La Jolla, CA, and approved August 19, 2016 (received for review May 25, 2016)

Mumps virus (MuV) remains an important pathogen worldwide, causing epidemic parotitis, orchitis, meningitis, and encephalitis. Here we show that MuV preferentially uses a trisaccharide containing α2,3-linked sialic acid in unbranched sugar chains as a receptor. Crystal structures of the MuV attachment protein hemagglutinin-neuraminidase (MuV-HN) alone and in complex with the α2,3-sialylated trisaccharide revealed that in addition to the interaction between the MuV-HN active site residues and sialic acid, other residues, including an aromatic residue, stabilize the third sugar of the trisaccharide. The importance of the aromatic residue and the third sugar in the MuV-HN–receptor interaction was confirmed by computational energy calculations, isothermal titration calorimetry studies, and glycan-binding assays. Furthermore, MuV-HN was found to bind more efficiently to unbranched α2,3-sialylated sugar chains compared with branched ones. Importantly, the strategically located aromatic residue is conserved among the HN proteins of sialic acid-using paramyxoviruses, and alanine substitution compromised their ability to support cell–cell fusion. These results suggest that not only the terminal sialic acid but also the adjacent sugar moiety contribute to receptor function for mumps and these paramyxoviruses. The distribution of structurally different sialylated glycans in tissues and organs may explain in part MuV's distinct tropism to glandular tissues and the central nervous system. In the crystal structure, the epitopes for neutralizing antibodies are located around the α-helices of MuV-HN that are not well conserved in amino acid sequences among different genotypes of MuV. This may explain the fact that MuV reinfection sometimes occurs.

structure | entry | receptor | infection | paramyxovirus

Mumps virus (MuV), an important aerosol-transmitted human pathogen, affects the parotid and other salivary glands, pancreas, testis, ovary, mammary glands, and kidney (1). It also infects the central nervous system, causing meningitis and, less frequently, encephalitis and unilateral nerve deafness. The hallmarks of MuV infection were described in the fifth century BC by Hippocrates (1). To prevent this disease, inactivated and live attenuated MuV vaccines were developed in 1946 and 1958, respectively (1). Currently, MuV vaccine is usually given as a live measles–mumps–rubella (MMR) vaccine. Although the cellular receptors and structures of viral glycoproteins, the main target of neutralizing antibodies (Abs), have been well characterized for measles and rubella viruses (2–4), the exact identity of a receptor for MuV and the crystal structure of its attachment glycoprotein remain to be determined. Although the MMR vaccine has dramatically reduced the prevalence of MuV infection (1), MuV vaccine-induced meningitis, a main adverse reaction, occurs at a rate ranging from 1/400 to 1/1,000,000 of vaccinated individuals, depending on the strain (1). Other studies have reported infection, as well as reinfection, among highly vaccinated populations (5, 6).

MuV is classified into 12 genotypes, which are used for surveillance by the World Health Organization (1). The vaccine strains currently used worldwide belong to genotype A, B, H, or N (1). Although MuV is thought to be serologically monotypic (1, 7), some studies have reported that MuV genotype-specific Abs are produced (8, 9). Thus, the antigenic variation among different genotypes is a concern for MuV vaccination and natural infection (5, 7).

MuV is a member of the genus *Rubulavirus* in the family *Paramyxoviridae*. Paramyxoviruses, enveloped and nonsegmented negative-strand RNA viruses, enter the host cell by attaching to a cell surface receptor via hemagglutinin-neuraminidase (HN), hemagglutinin (H), or glycoprotein (G), depending on the virus, and cause membrane fusion through the action of the fusion (F) protein (10). The attachment proteins (HN, H, and G) are the major targets of neutralizing Abs, along with the F protein (1). The MuV genome contains 15,384 nucleotides encoding nucleocapsid, phospho, matrix, F, small hydrophobic, HN, and large proteins (1). Sialic acid, expressed on the cell surface as a nonreducing terminal component of sugar chains, is believed to be the common receptor for many paramyxoviruses including MuV, and influenza viruses (10, 11). Human and avian influenza viruses

Significance

Despite the availability of an effective vaccine, mumps virus (MuV) still causes outbreaks even in highly vaccinated populations worldwide. MuV affects the salivary glands, testicles, ovaries, pancreas, meninges, and brain. This characteristic tropism to glandular tissues and the central nervous system remains to be explained. Here, using X-ray crystallography, computational energy calculations, isothermal titration calorimetry, glycan-binding assays, and MuV glycoprotein-mediated cell fusion assays, we show that the trisaccharide containing an α2,3-linked sialic acid on the cell surface acts as a receptor for MuV. In conjunction with elucidation of the distribution of structurally different sialylated glycans in tissues and organs, this finding will lead to a better understanding of MuV tropism and pathogenesis.

Author contributions: M.K., K.T., Y.Y., and T.H. designed research; M.K., K.T., S.W., S.O., R.M., S.-i.N., H.H., T.N., T.T., N.S., M.S., and T.H. performed research; M.K., K.T., R.M., D.K., S.-i.N., H.H., Y.S., T.N., T.T., K.S., N.S., M.S., Y.Y., and T.H. analyzed data; and M.K., Y.Y., and T.H. wrote the paper.

The authors declare no conflict of interest.

This article is a PNAS Direct Submission.

Data deposition: The atomic coordinates and structure factors have been deposited in the Protein Data Bank, www.wwpdb.org [PDB ID codes 5B2C (MuV-HN) and 5B2D (MuV-HN−3′-SL)].

[1]To whom correspondence may be addressed. Email: ktakeuch@md.tsukuba.ac.jp or takaoh@virology.med.kyushu-u.ac.jp.

This article contains supporting information online at www.pnas.org/lookup/suppl/doi:10.1073/pnas.1608383113/-/DCSupplemental.

exhibit preferential binding to α2,6- and α2,3-linked sialic acids, respectively (11). The distinct preference for either of the two major types of sialic acid is an important determinant of the influenza virus host range (11). Whether MuV uses a particular sialylated sugar structure as a receptor is unknown.

In this study, we first determined the crystal structures of the MuV-HN protein (hereinafter abbreviated as MuV-HN) receptor-binding head domain alone and in complex with trisaccharides containing sialic acid. Based on the structures thus obtained, we further examined the MuV-HN–receptor interaction using computational calculations, isothermal titration calorimetry (ITC) studies, glycan-binding assays, and functional studies. The structures of MuV-HN also provided important insights into the mechanism of Ab-mediated neutralization.

Results

Overall Structures of the MuV-HN Head Domain Alone and in Complex with Sialyllactose. MuV-HN comprises an N-terminal cytoplasmic tail, transmembrane region, stalk, and C-terminal receptor-binding head domain (1). To gain insight into the MuV–receptor interaction, we determined the crystal structure of MuV-HN. The HN head domain of the MuV Hoshino strain was expressed in HEK293S cells lacking *N*-acetylglucosaminyltransferase I [293S GnTI(−) cells], which allows glycoproteins to possess homogeneously modified glycans and thus aids in the production of better-diffracting crystals (12). The purified MuV-HN head domain was methylated following a previously developed method (13) and crystallized. Diffraction to 2.24-Å resolution was obtained for a single crystal of the MuV-HN head domain. Its structure was determined by molecular replacement using Newcastle disease virus-HN (14) as a search model and was refined to an R_{work} value of 20.2% and an R_{free} value of 22.2% (Table S1). In addition, the MuV-HN head domain was cocrystallized with two types of sialyllactose, 3′-sialyllactose (3′-SL) and 6′-sialyllactose (6′-SL), as the sialic acid-containing receptor analogs. These are trisaccharides in which the terminal *N*-acetylneuraminic acid (hereinafter referred to as Sia-1) is connected to the galactosyl unit (referred to as Gal-2) of lactose by the α2,3-linkage and the α2,6-linkage, respectively. (The glucose unit of lactose is referred to as Glc-3.) The cocrystal structure with 3′-SL was determined at 2.18-Å resolution and was refined to an R_{work} value of 17.6% and an R_{free} value of 19.1% (Table S1). Two monomers are contained in the asymmetric unit of both free and 3′-SL–bound forms of the MuV-HN head domain.

The MuV-HN head domain exhibits a six-bladed β-propeller fold (β1–β6 sheets) and forms a homodimer (Fig. 1 *A* and *B*). The two monomers forming a dimer are tilted approximately 90° to each other. Similar to attachment proteins of other paramyxoviruses (14–17), two dimers form a tetramer (dimer of dimers) (Fig. S1*A*). The ligand 3′-SL is bound to the top pocket of the MuV-HN head domain (Fig. 1*B* and Fig. S1*A*). In the homodimer, no large structural difference is observed between the free and receptor-bound forms of the MuV-HN head domain (rmsd of 0.40 Å; 882 Cα atoms in the dimer) (Fig. S1*B*).

The structure of the MuV-HN head domain cocrystallized with 6′-SL was also determined. However, the electron density for 6′-SL was not detected in the structure, suggesting that MuV-HN does not efficiently bind 6′-SL.

Interaction of MuV-HN and 3′-SL. In the crystal structure of MuV-HN complexed with 3′-SL, the aromatic residues Tyr268 and Phe370 are stacked together with Tyr369, which interacts face to face with Glc-3 of 3′-SL. The O^{η} oxygen atom of Tyr369 hydrogen bonds with the O1 oxygen atom of Glc-3 and the O1 oxygen atom of Gal-2 (Fig. 1*C*, *Left*). Furthermore, Val476 stabilizes Glc-3 by hydrogen bonding through its main chain with the O6 oxygen atom of the sugar, and by forming a hydrophobic interaction with Glc-3 through its side chain. Notably, Tyr369, and Val476 are conserved among all genotypes of MuV, but they are not among the seven active site residues highly conserved in viral and cellular sialidases, which are responsible for sialic acid recognition (18). The active site residues correspond to Arg180, Glu407, Arg422, Arg512, Tyr540, Glu561, and Asp204 in the HN proteins of MuV, and these seven residues are, as expected, conserved among all genotypes of MuV. The first five of these residues are involved in the direct binding to Sia-1 of 3′-SL, and

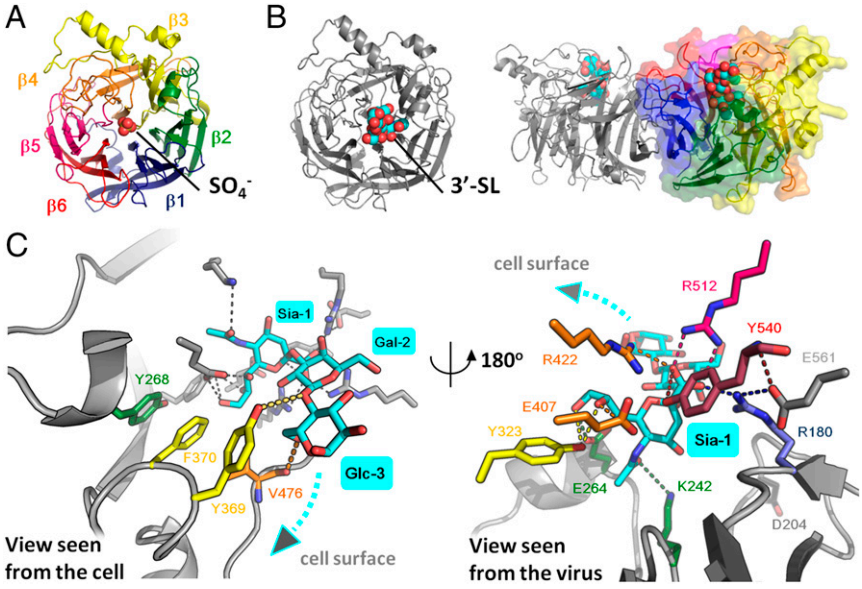

Fig. 1. Structures of the MuV-HN head domain. (*A*) Top view of the MuV-HN monomer in the absence of receptor whose β-sheets (β1–β6) are rainbow in color. The SO_4^- ion is shown in spheres. (*B*) MuV-HN monomer (*Left*, top view) and homodimer (*Right*, side view) bound to 3′-SL. 3′-SL is shown in spheres. (*C*) MuV-HN residues involved in receptor binding. The MuV-HN residues involved in the interaction with Glc-3 and Gal-2 of 3′-SL (cyan) (*Left*, view seen from the cell) and with Sia-1 of 3′-SL (*Right*, view seen from the virus) are indicated by the same rainbow colors as in *A*. The other active site residues, E561 and D204, conserved among paramyxoviruses, are colored in gray. Nitrogen atom, blue; oxygen atom, red.

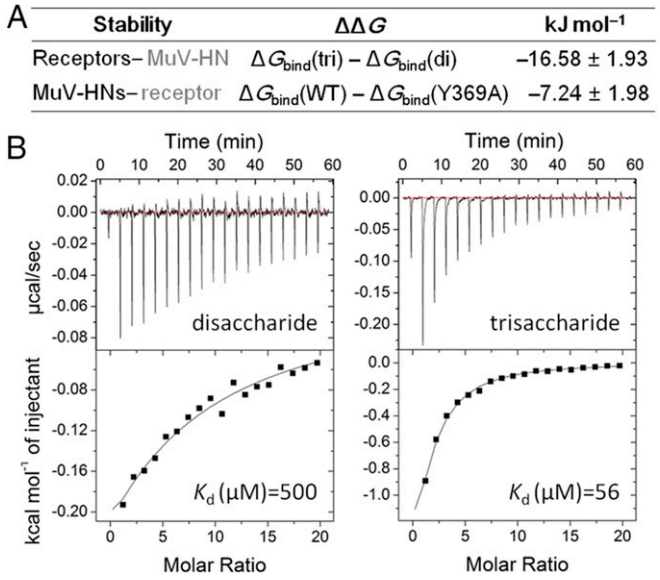

Fig. 2. Stability of the MuV HN protein-receptor complex. (*A*) The energetic stability of the HN protein–receptor interaction calculated with the MD simulations. di, disaccharide; tri, trisaccharide. (*B*) ITC analysis of the binding of glycans to the MuV-HN protein. (*Upper*) Raw titration data. (*Lower*) Integration plot of the titration data. (*Left*) MuV-HN protein–NeuAcα2,3Gal (disaccharide). (*Right*) MuV-HN protein–NeuAcα2,3Galβ1,4Glc (trisaccharide).

Lys242, Glu264, and Tyr323 also bind to Sia-1, along with the five residues (Fig. 1*C*, *Right*). Glu561 appears to support the conformations of the side chain of Arg180 and the main chain of Tyr540, but does not appear to be involved in direct binding to Sia-1. Another active site residue, Asp204, points away from Sia-1 and does not contribute to HN's interaction with it (Fig. 1*C*, *Right*). In the absence of 3′-SL, an SO_4^- ion is observed within the top pocket of the MuV-HN head domain under the crystallization condition in which the crystallization buffer contains sulfate (Fig. 1*A*). In MuV-HN cocrystallized with 3′-SL, the ion's density disappears and is replaced by 3′-SL (Fig. 1*B*). In the human body, a PO_4^- ion instead of an SO_4^- ion may be present at that position, so that the HN protein is stabilized before it binds to a receptor.

The foregoing observations suggested to us that the saccharide moiety underlying the terminal sialic acid also plays an important role in the MuV HN–receptor interaction.

Stability of the HN Protein–Receptor Interaction. In an attempt to evaluate the energetic stability of the MuV-HN protein-receptor complex, we first compared sialic acid-containing trisaccharides and disaccharides for their ability to interact with MuV-HN based on molecular dynamics (MD) simulations. Computational calculations revealed that the trisaccharide 3′-SL exhibits more stable binding to MuV-HN ($\Delta\Delta G = -16.58 \pm 1.93$ kJ/mol) than the disaccharide Sia-1–Gal-2 (Fig. 2*A* and Fig. S2*A*). We also compared energetic stability in the wild type (WT) of MuV-HN and its mutant in which Tyr-369 was replaced with Ala (Y369A). Our calculations showed that the WT binds more stably to 3′-SL ($\Delta\Delta G = -7.24 \pm 1.98$ kJ/mol) compared with the mutant (Fig. 2*A* and Fig. S2*B*). These results support the idea that the third sugar of 3′-SL and Tyr369 of MuV-HN contribute substantially to the MuV HN–receptor interaction.

We also examined the binding affinity of the MuV-HN protein receptor using ITC studies. Consistent with the computational calculations, the trisaccharide 3′-SL exhibited much stronger binding affinity to the MuV-HN protein ($K_d = 56$ μM) compared with the disaccharide Sia-1–Gal-2 ($K_d = 500$ μM) (Fig. 2*B*).

MuV-HN Preferentially Binds to Oligosaccharides Containing α2,3-Linked Sialic Acid. We next examined the binding of MuV-HN to six types of glycans containing α2,3- or α2,6-linked sialic acid (G1–G6 in Fig. 3*A*) using a glycoconjugate-spotted microplate (19, 20). The glycoconjugates represent major sialylated glycans found in the human respiratory tract (21), and their structural compositions are described in Fig. 3*A*. Fluorescence due to the binding of MuV-HN was observed for G1 and less strongly for G2 (Fig. 3*A*). G1 and G2 are glycans containing α2,3-linked sialic acid. Only a limited amount of fluorescence was observed for G3 and glycans containing α2,6-linked sialic acid, including G4, G5, and G6. On a different plate containing sialylated and non-sialylated glycans (22), MuV-HN was found to exhibit binding to NeuAcα2,3Galβ1,4Glc-BSA and NeuAcα2,3Galβ1,4GlcNAc-polyglutamine, but only low levels of binding to the other glycans examined (Fig. S3). We also tested the binding of the MuV-HN Y369A mutant to NeuAcα2,3Galβ1,4GlcNAc-polyglutamine and NeuAcα2,3Galβ1,4Glc-BSA (Fig. 3*B*). The mutant exhibited a

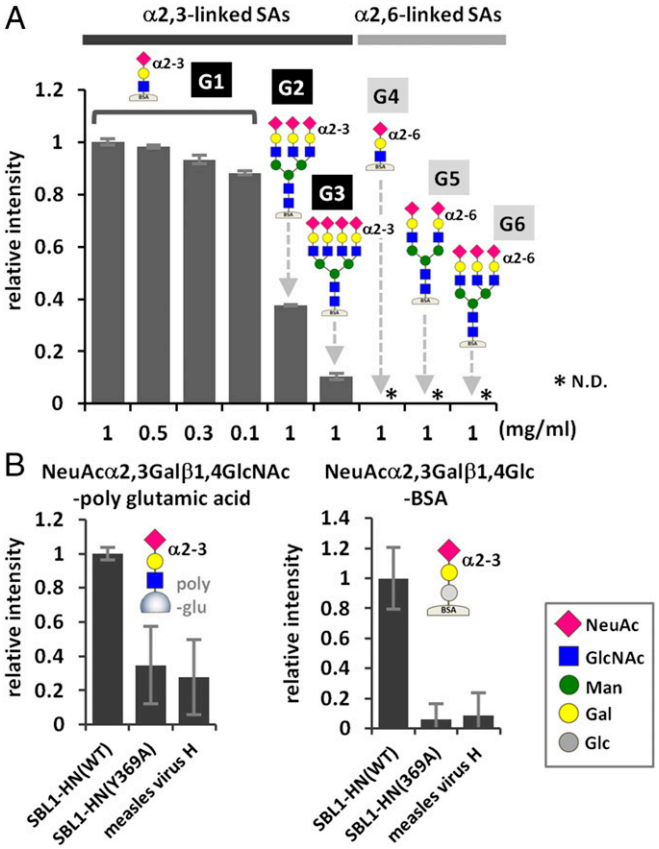

Fig. 3. Binding of MuV-HN proteins to sialyl glycans. (*A*) Binding of purified MuV-HN protein to six branched/unbranched α2,3- or α2,6-linked sialyl glycans. G1, NeuAcα2,3Galβ1,4GlcNAc-BSA; G2, NeuAcα2,3Galβ1,4GlcNAc β1,2(NeuAcα2,3Galβ1,4GlcNAcβ1,4)Manα1,3(NeuAcα2,3Galβ1,4GlcNAcβ1,2Manα1,6)Manβ1,4GlcNAcβ1,4GlcNAc-BSA; G3, NeuAcα2,3Galβ1,4GlcNAcβ1,2(NeuAcα2,3Galβ1,4GlcNAcβ1,4)Manα1,3(NeuAcα2,3Galβ1,4GlcNAcβ1,2 (NeuAcα2,3Galβ1,4GlcNAcβ1,6)Manα1,6)Manβ1,4GlcNAcβ1,4GlcNAc-BSA; G4, NeuAcα2,6Galβ1,4GlcNAc-BSA; G5, NeuAcα2,6Galβ1,4GlcNAcβ1,2Manα1,3(NeuAcα2,6Galβ1,4GlcNAcβ1,2Manα1,6)Manβ1,4GlcNAcβ1,4GlcNAc-BSA; G6, NeuAcα2,6Galβ1,4GlcNAcβ1,2(NeuAcα2,6Galβ1,4GlcNAcβ1,4)Manα1,3 (NeuAcα2,6Galβ1,4GlcNAcβ1,2Manα1,6)Manβ1,4GlcNAcβ1,4GlcNAc-BSA. The glycans are attached onto BSA. (*B*) Binding of purified MuV-HN proteins, WT or Y369A, to the trisaccharides NeuAcα2,3Galβ1,4GlcNAc-polyglutamic acid (*Left*) and NeuAcα2,3Galβ1,4Glc-BSA (*Right*). Measles virus H protein served as a negative control. Data are the mean ± SD of three samples. N.D., not detected. Data shown in this figure are representative of three independently performed experiments.

decreased level of binding to both glycans containing α2,3-linked sialic acid compared with the WT.

In the foregoing studies, the HN protein (amino acid positions 96–582) of the MuV SBL-1 strain (genotype A) was used. We also examined the binding of mumps virions of the SBL-1, Tokyo M-21 (genotype G), and Tokyo S-III-10 (genotype L) strains (23), as well as the purified HN protein of the MuV Hoshino strain (genotype B), to α2,3- and α2,6-linked sialyl glycopolymers (Neu5Acα2,3Galβ1,4GlcNAcβ-pAP and Neu5Acα2,6Galβ1,4GlcNAcβ-pAP) (24) on microplates. All MuV particles examined bound to α2,3-linked sialyl glycopolymers, but not to α2,6-linked sialyl glycopolymers (Fig. S4).

These binding assays indicate that MuV-HN preferentially binds to oligosaccharides containing α2,3-linked sialic acid, and that branching of saccharides tends to decrease the binding. The results also reveal that Tyr369 in MuV-HN, which interacts with the third sugar (Glc-3) of 3′-SL (Fig. 1*C*, *Left*), is critical for the binding of MuV HN to oligosaccharides containing α2,3-linked sialic acid.

α2,3-Linked Sialic Acid Is Necessary for MuV-Mediated Cell–Cell Fusion and Entry. To evaluate the importance of α2,3-linked sialic acid in MuV receptor function, we cleaved α2,3-linked sialic acid from the cell surface using sialidases. The amounts of α2,3- and α2,6-linked sialic acids on HEK293 cells, as evaluated by flow cytometry, were close to the background levels after treatment with *Arthrobacter ureafaciens* sialidase, which cleaves both the α2,3 and α2,6 linkages of *N*-acetylneuraminic acid (Fig. S5*A*). The α2,3- and α2,6-linked sialic acids were detected by binding to the *Maackia amurensis* lectin II (MAL II) and *Sambucus nigra* agglutinin (SNA), respectively. Treatment with *Salmonella typhimurium* α2,3-sialidase also resulted in lower levels of α2,3-linked sialic acid on the cell surface, although the reduction was not as complete as that seen with *A. ureafaciens* sialidase. As expected, the amount of α2,6-linked sialic acid on the cell surface was not affected by treatment with α2,3-sialidase.

We next performed a fusion assay to assess the effect of sialic acid cleavage on cell–cell fusion mediated by MuV HN and F proteins. HEK293 cells were transiently transfected with the expression plasmid encoding EGFP. These HEK293-EGFP cells were then treated with α2,3-sialidase, *A. ureafaciens* sialidase, or control medium. HEK293 cells in different dishes were transfected with the expression plasmids encoding HN and F proteins of MuV. After 20 h of sialidase treatment, HEK293-EGFP cells were overlaid onto HEK293 cells expressing MuV HN and F proteins (Fig. S5*B*). If HEK293-EGFP cells (treated or untreated with sialidases) fuse with HEK293 cells expressing the HN and F proteins, then EGFP-positive syncytia will be observed. EGFP-positive syncytia were clearly detected at 15 min after the overlay in the control cell mixture containing sialidase-untreated HEK293-EGFP cells, but not in the cell mixture containing α2,3-sialidase–treated or *A. ureafaciens* sialidase-treated HEK293-EGFP cells (Fig. 4*A*). The size and number of EGFP-expressing syncytia increased gradually with time (at 30 and 60 min) in the control cell mixture. In contrast, the cell mixture containing α2,3-sialidase–treated or *A. ureafaciens* sialidase-treated HEK293-EGFP cells formed a reduced number of small EGFP-expressing syncytia at 30 min or 60 min after overlay, respectively. Residual and/or regenerated (or recycled) α2,3-linked sialic acid on sialidase-treated HEK293-EGFP cells presumably supported syncytium formation in these cell mixtures at later time points. The same results were obtained with the respiratory epithelial cell line NCI-H358 or the neuroblastoma cell line IMR-32 when these cells instead of HEK293 cells were transfected with EGFP, treated with sialidases and overlaid onto HEK293 expressing MuV HN and F proteins (Fig. S5 *A*, *C*, and *D*). Sialidase treatment had no affect on the cell–cell fusion mediated by the H and F proteins of the measles virus, owing to the proteinaceous nature of the receptors (Fig. S5*E*).

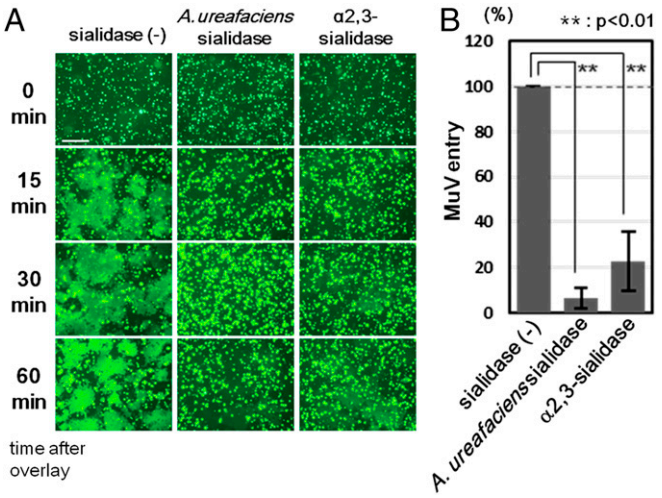

Fig. 4. Effect of cleavage of sialic acid on MuV-induced cell–cell fusion and MuV entry. (*A*) HEK293 cells expressing EGFP were treated with control medium, α2,3-sialidase, or *A. ureafaciens* sialidase. They were detached from the plates and then overlaid onto HEK293 cells expressing the HN and F proteins of MuV. The cells were observed under fluorescence microscopy at 0, 15, 30, and 60 min after overlay. (Scale bar: 200 μm.) (*B*) HEK293 cells pretreated with control medium, α2,3-sialidase, or *A. ureafaciens* sialidase were infected with the EGFP-expressing recombinant MuV. At 24 h post-infection, EGFP-positive cells were counted to evaluate the efficiency of virus entry. The control was set to 100, and data indicate the mean ± SD of triplicate experiments. The data are representative of three independently performed experiments. $^{**}P < 0.01$, two-tailed Student's *t* test.

We also examined MuV entry into sialidase-treated cells. HEK293 cells that had been treated with α2,3-sialidase, *A. ureafaciens* sialidase, or control medium were infected with EGFP-expressing recombinant MuV. Entry efficiencies in α2,3-sialidase–treated and *A. ureafaciens* sialidase-treated HEK293 cells were 20% and ∼8%, respectively, of that seen in control cells (Fig. 4*B*).

Interaction of the HN Protein with the Third Sugar from the Nonreducing Terminal of Saccharide Also Contributes to Paramyxovirus-Mediated Cell–Cell Fusion. Given that our structural and binding studies indicated the involvement of Glc-3 at the base of the terminal sialic acid in the interaction with MuV-HN, we examined the functional role of this third sugar of the trisaccharide. HEK293 cells were transfected with the expression plasmid encoding the HN protein of the MuV Hoshino strain or its mutant with the Y369A substitution (Fig. 5*A*, *Left*), together with the expression plasmids encoding the MuV F protein and EGFP, respectively. The mutant HN protein was expressed on the cell surface as efficiently as the WT protein, as assessed by flow cytometry (Fig. S6*A*). The cells transfected with the mutant HN protein apparently produced a lower level of cell–cell fusion compared with cells transfected with the WT HN protein (Fig. 5*A*, *Right*). The same results were obtained with NCI-H358 and IMR-32 cells (Fig. S6*B*).

To test whether this finding would also hold true for other paramyxoviruses using sialic acid as a receptor, we examined HN proteins of parainfluenza virus 5 (PIV5), human parainfluenza virus 2 (PIV2), and Sendai virus (SeV). PIV5 and PIV2, like MuV, belong to the genus *Rubulavirus*, whereas SeV is a member of the genus *Respirovirus*. The structures of the PIV5 HN protein unbound and bound to the receptor have been determined (16), but those of the PIV2 and SeV HN proteins have not; therefore, we generated the model structures for the HN proteins of the latter two viruses based on the known HN structures of other

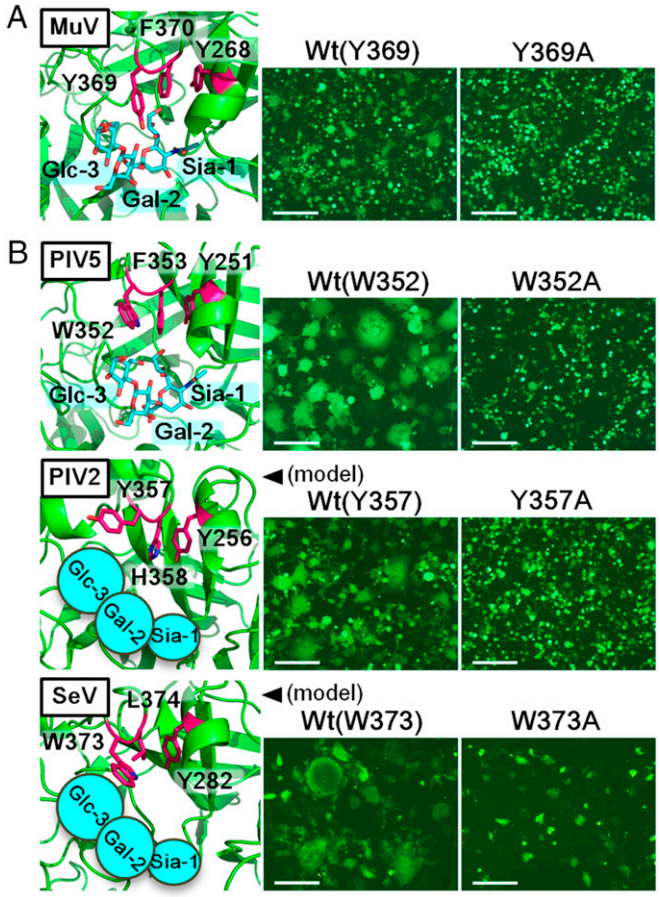

Fig. 5. Involvement of the third sugar from the nonreducing terminal in the HN protein–receptor interaction. Experiments were performed for the HN protein of MuV (*A*) and PIV5, PIV2, and SeV (*B*). (*Left*) Aromatic residues involved in the interaction with the third sugar from the nonreducing terminal (Glc-3 of SL) as well as residues stacked with them in solved (MuV and PIV5) or model HN protein structures (PIV2 and SeV) are shown in magenta. SLs (Sia-1, Gal-2, and Glc-3) are shown in cyan. (*Right*) HEK293 (MuV, PIV5, and PIV2) or Vero (SeV) cells transfected with expression plasmids encoding the HN protein (WT or mutant), F protein, and EGFP were observed for syncytia formation using fluorescence microscopy at 2 d posttransfection. (Scale bar: 200 μm.)

paramyxoviruses, including PIV5 and PIV3 (16, 17). These solved and model structures show that Trp352, Tyr357, and Trp373 of PIV5, PIV2, and SeV HN proteins, respectively, interact with Glc-3 of sialyllactose (Fig. 5*B*, *Left*), similar to Tyr369 of MuV-HN. We mutated these residues to alanine and then tested the ability of the mutant HN proteins to support cell–cell fusion in conjunction with the corresponding F proteins. All of the mutant HN proteins were expressed on the cell surface as efficiently as the WT proteins (Fig. S6*A*), but induced cell fusion much less efficiently (Fig. 5*B*). These results indicate that in addition to the terminal sialic acid, the third sugar from the nonreducing terminal contributes to the HN protein–receptor interaction. (The structures suggest that the fourth sugar, rather than the third sugar, from the nonreducing terminal may interact with the aromatic residues of PIV5 and PIV2.)

Discussion

It is generally believed that the sialic acid on glycans is a receptor for paramyxoviruses belonging to the genera *Respirovirus*, *Rubulavirus*, and *Avulavirus* (10), but whether structures other than the terminal sialic acid are directly involved in the interaction with the HN proteins of these paramyxoviruses is unknown. Our findings indicate that the third sugar from the nonreducing terminal of glycans also contributes to the receptor–HN protein interaction in MuV, and that a trisaccharide containing α2,3-linked sialic acid is the core structure of a receptor for MuV.

In the X-ray crystal structures, the electron density of the trisaccharide was detected in the MuV-HN head domain cocrystalized with 3′-SL, but not in that cocrystallized with 6′-SL. Importantly, the crystal structures revealed that the binding of 3′-SL to MuV-HN not only is mediated by the MuV-HN–sialic acid interaction, but also is stabilized by the interaction between Gal-2/Glc-3 of 3′-SL and Tyr369/Val476 of MuV-HN. The stacking interaction of Tyr369 with the adjacently located Phe370 and Tyr268 also may contribute to the stability of the interaction with Glc-3. The Y369A substitution considerably reduced cell–cell fusion mediated by the HN and F proteins. Because the Y369A substitution is unlikely to dramatically affect the conformation of the MuV-HN monomer, the conformation of the dimer, or the orientation of the tetramer, the lack of interaction between MuV-HN and Glc-3 must be the reason for the reduced cell–cell fusion. Computational calculations using the MD simulations and binding-affinity evaluation by ITC also support the importance of both the aromatic residue at this position of MuV-HN and the third sugar from the nonreducing terminal of the trisaccharide for the stability of the MuV-HN–sugar complex. The importance of the third sugar–HN aromatic residue interaction also appears to apply to the paramyxoviruses PIV5, PIV2, and SeV. Thus, we may have to reconsider the structural properties of receptors for other sialic acid-using viruses as well.

The finding that MuV-HN favors α2,3-linked sialic acid over α2,6-linked sialic acid was supported by the results of glycan binding assays and cell–cell fusion studies after sialidase treatment. The 3′-SL (used for crystal studies and the glycan-binding assay) may constitute the terminal structure of glycosphingolipids, whereas 3′-sialyllactosamine (used for the glycan binding assay) exists as the terminal sugar of *N*-linked and *O*-linked glycoproteins (25). The sole difference between these trisaccharides is the acetylation of Glc-3 in the latter. The binding of MuV-HN to both types of sugars suggests that MuV could use glycosphingolipids and/or glycoproteins as receptors (Fig. 3*B* and Fig. S4). The crystal structure of MuV-HN bound to 3′-SL also suggests that the acetylation of Glc-3 does not spatially inhibit the interaction of the trisaccharide containing α2,3-linked sialic acid with Tyr369 and other residues of MuV-HN. Because the MuV-HN residues involved in the interaction with 3′-SL are highly conserved, the trisaccharide containing the α2,3-linked sialic acid is likely essential for all genotypes of MuV. In fact, MuV strains of the genotypes A, B, G, and L all exhibited a preference for glycans containing α2,3-linked sialic acid, although genotype A has different antigenicity than the others (23).

Interestingly, MuV-HN bound more strongly to the simple α2,3-sialylated trisaccharide than to the branched α2,3-sialylated oligosaccharides, and its binding was weaker to a tetra-antennary complex glycan than to a triantennary complex glycan. The results suggest that additional sugars at the base of the sialylated trisaccharide may affect the interaction with MuV-HN via steric hindrance. Sialylated glycans have highly diverse structures and compositions (25). It has been shown that α2,6- and α2,3-linked sialic acids are largely present in the upper and lower respiratory tracts in humans, respectively (11); however, the systemic distribution of structurally different glycans in tissues and organs remains to be adequately characterized. A more detailed study may shed light on MuV's distinct tropism to glandular tissues and the central nervous system.

The crystal structure of MuV-HN also provides insight into the mechanism by which Abs induced by natural infection and vaccination neutralize MuV. When mapped on the structure of

MuV-HN, the great majority of the reported epitopes of anti–MuV-HN Abs (8, 26, 27) are located around α-helices A (positions 264–269), B (positions 331–336), and C (positions 354–365) of the MuV-HN head domain (Fig. S7). Helices A, B, and C correspond to α1, α3, and α4, respectively, in the Newcastle disease virus HN protein (14). Interestingly, the similarly positioned α-helix is known as the hemagglutinin noose epitope (HNE; residues at positions 379–410) in measles virus H (28). Given that these epitopes on α-helices (helices A, B, and C on MuV-NH and HNE on measles virus H) apparently are not involved in receptor binding (15, 29), Abs against them are likely to neutralize the viruses by mechanisms other than the inhibition of receptor binding. Whereas amino acid residues in the HNE region of measles virus H are highly conserved (28), those of the MuV-HN α-helices exhibit diversity among the different genotypes of MuV (Fig. S7, *Right*). Although MuV has been considered serologically monotypic (1, 7), genotype-specific neutralizing Abs against MuV-HN can be produced at polyclonal levels (8, 9). Thus, the amino acid variability in the neutralizing epitopes may be an explanation, along with waning immunity, for the recent reports of MuV infection and reinfection among vaccinated and naturally infected populations, respectively (5, 6).

Materials and Methods

HEK293, IMR-32, and Vero cells were maintained in DMEM (Wako) supplemented with 10% (vol/vol) FBS (Sigma-Aldrich) and penicillin/streptomycin (Gibco). NCI-H358 cells were maintained in RPMI medium (Wako) supplemented with 10% (vol/vol) FBS and penicillin/streptomycin. The expression, purification, crystallization, and structure determination of proteins were carried out as described previously (15, 29), with some modifications. The MD simulation was performed with Gromacs 5.0.5 (30). The free energy values were calculated with the g_bar module of Gromacs. ITC experiments were performed using a MicroCal Auto-iTC200 calorimeter (Malvern Instruments). Binding constants were obtained by fitting the plots with a 1:1 binding model using Origin 7 (OriginLab). More detailed information is provided in *SI Materials and Methods*.

ACKNOWLEDGMENTS. We thank the beamline staff of Photon Factory (Tsukuba, Japan) for technical help during data collection, M. Tsurudome (Mie University) for the plasmids of PIV5 and PIV2, and T. Sakaguchi (Hiroshima University) for the plasmid of SeV. This study was supported by the Ministry of Education, Culture, Sports, Science, and Technology in Japan [Kakenhi Grants 26713018 (to T.H.) and 24115005 (to Y.Y.)], the Japan Society for the Promotion of Science [Postdoctoral Fellowship DC2 (to M.K. and R.M.)], the Uehara Memorial Foundation (T.H.), the Japan Foundation for Pediatric Research (T.H.), and the Takeda Science Foundation (T.H.). This study was partially supported by the Research Program on Emerging and Reemerging Infectious Diseases and the Platform Project for Supporting in Drug Discovery and Life Science Research (Platform for Drug Discovery, Informatics and Structural Life Science) from the Japan Agency for Medical Research and Development.

1. Rubin SA, Sauder CJ, Carbone KM (2013) Mumps virus. *Fields Virology*, eds Knipe DM, et al. (Lippincott Williams & Wilkins, Philadelphia), 6th Ed, Vol I, pp 1024–1041.
2. Griffin DE (2013) Measles virus. *Fields Virology*, eds Knipe DM, et al. (Lippincott Williams & Wilkins, Philadelphia), 6th Ed, Vol I, pp 1042–1069.
3. Cong H, Jiang Y, Tien P (2011) Identification of the myelin oligodendrocyte glycoprotein as a cellular receptor for rubella virus. *J Virol* 85(21):11038–11047.
4. DuBois RM, et al. (2013) Functional and evolutionary insight from the crystal structure of rubella virus protein E1. *Nature* 493(7433):552–556.
5. Latner DR, Hickman CJ (2015) Remembering mumps. *PLoS Pathog* 11(5):e1004791.
6. Yoshida N, et al. (2008) Mumps virus reinfection is not a rare event confirmed by reverse transcription loop-mediated isothermal amplification. *J Med Virol* 80(3): 517–523.
7. Rubin SA, et al. (2012) Recent mumps outbreaks in vaccinated populations: No evidence of immune escape. *J Virol* 86(1):615–620.
8. Örvell C, Alsheikhly AR, Kalantari M, Johansson B (1997) Characterization of genotype-specific epitopes of the HN protein of mumps virus. *J Gen Virol* 78(Pt 12): 3187–3193.
9. Rydbeck R, Löve A, Örvell C, Norrby E (1986) Antigenic variation of envelope and internal proteins of mumps virus strains detected with monoclonal antibodies. *J Gen Virol* 67(Pt 2):281–287.
10. Lamb RA, Parks GD (2013) Paramyxoviridae. *Fields Virology*, eds Knipe DM, et al. (Lippincott Williams & Wilkins, Philadelphia), 6th Ed, Vol I, pp 957–995.
11. Wright PF, Neumann G, Kawaoka Y (2013) Orthomyxoviruses. *Fields Virology*, eds Knipe DM, et al. (Lippincott Williams & Wilkins, Philadelphia), 6th Ed, Vol I, pp 1186–1243.
12. Reeves PJ, Callewaert N, Contreras R, Khorana HG (2002) Structure and function in rhodopsin: High-level expression of rhodopsin with restricted and homogeneous N-glycosylation by a tetracycline-inducible N-acetylglucosaminyltransferase I-negative HEK293S stable mammalian cell line. *Proc Natl Acad Sci USA* 99(21):13419–13424.
13. Walter TS, et al. (2006) Lysine methylation as a routine rescue strategy for protein crystallization. *Structure* 14(11):1617–1622.
14. Crennell S, Takimoto T, Portner A, Taylor G (2000) Crystal structure of the multifunctional paramyxovirus hemagglutinin-neuraminidase. *Nat Struct Biol* 7(11): 1068–1074.
15. Hashiguchi T, et al. (2007) Crystal structure of measles virus hemagglutinin provides insight into effective vaccines. *Proc Natl Acad Sci USA* 104(49):19535–19540.
16. Yuan P, et al. (2005) Structural studies of the parainfluenza virus 5 hemagglutinin-neuraminidase tetramer in complex with its receptor, sialyllactose. *Structure* 13(5): 803–815.
17. Lawrence MC, et al. (2004) Structure of the haemagglutinin-neuraminidase from human parainfluenza virus type III. *J Mol Biol* 335(5):1343–1357.
18. Colman PM, Hoyne PA, Lawrence MC (1993) Sequence and structure alignment of paramyxovirus hemagglutinin-neuraminidase with influenza virus neuraminidase. *J Virol* 67(6):2972–2980.
19. Nakakita S, Hirabayashi J (2016) Preparation of glycan arrays using pyridylaminated glycans. *Methods Mol Biol* 1368:225–235.
20. Imamura T, et al. (2014) Antigenic and receptor binding properties of enterovirus 68. *J Virol* 88(5):2374–2384.
21. Walther T, et al. (2013) Glycomic analysis of human respiratory tract tissues and correlation with influenza virus infection. *PLoS Pathog* 9(3):e1003223.
22. Tateno H, et al. (2008) Glycoconjugate microarray based on an evanescent-field fluorescence-assisted detection principle for investigation of glycan-binding proteins. *Glycobiology* 18(10):789–798.
23. Inou Y, et al. (2004) Molecular epidemiology of mumps virus in Japan and proposal of two new genotypes. *J Med Virol* 73(1):97–104.
24. Totani K, et al. (2003) Chemoenzymatic synthesis and application of glycopolymers containing multivalent sialyloligosaccharides with a poly(L-glutamic acid) backbone for inhibition of infection by influenza viruses. *Glycobiology* 13(5):315–326.
25. Varki A, et al. (2009) *Essentials of Glycobiology* (Cold Spring Harbor, New York), 2nd Ed.
26. Kövamees J, Rydbeck R, Orvell C, Norrby E (1990) Hemagglutinin-neuraminidase (HN) amino acid alterations in neutralization escape mutants of Kilham mumps virus. *Virus Res* 17(2):119–129.
27. Cusi MG, et al. (2001) Localization of a new neutralizing epitope on the mumps virus hemagglutinin-neuraminidase protein. *Virus Res* 74(1-2):133–137.
28. Ziegler D, et al. (1996) Protection against measles virus encephalitis by monoclonal antibodies binding to a cystine loop domain of the H protein mimicked by peptides which are not recognized by maternal antibodies. *J Gen Virol* 77(Pt 10):2479–2489.
29. Hashiguchi T, et al. (2011) Structure of the measles virus hemagglutinin bound to its cellular receptor SLAM. *Nat Struct Mol Biol* 18(2):135–141.
30. Hess B, Kutzner C, van der Spoel D, Lindahl E (2008) GROMACS 4: Algorithms for highly efficient, load-balanced, and scalable molecular simulation. *J Chem Theory Comput* 4(3):435–447.
31. Ninomiya K, et al. (2009) Amino acid substitution at position 464 in the haemagglutinin-neuraminidase protein of a mumps virus Urabe strain enhanced the virus growth in neuroblastoma SH-SY5Y cells. *Vaccine* 27(44):6160–6165.
32. Rawling J, García-Barreno B, Melero JA (2008) Insertion of the two cleavage sites of the respiratory syncytial virus fusion protein in Sendai virus fusion protein leads to enhanced cell-cell fusion and a decreased dependency on the HN attachment protein for activity. *J Virol* 82(12):5986–5998.
33. Kabsch W (2010) XDS. *Acta Crystallogr D Biol Crystallogr* 66(Pt 2):125–132.
34. McCoy AJ, et al. (2007) Phaser crystallographic software. *J Appl Cryst* 40(Pt 4):658–674.
35. Adams PD, et al. (2010) PHENIX: A comprehensive Python-based system for macromolecular structure solution. *Acta Crystallogr D Biol Crystallogr* 66(Pt 2):213–221.
36. Emsley P, Cowtan K (2004) Coot: Model-building tools for molecular graphics. *Acta Crystallogr D Biol Crystallogr* 60(Pt 12 Pt 1):2126–2132.
37. Case DA, et al. (2012) *AMBER 12 Reference Manual* (University of California San Francisco, San Francisco).
38. Kirschner KN, et al. (2008) GLYCAM06: A generalizable biomolecular force field. Carbohydrates. *J Comput Chem* 29(4):622–655.
39. Bennett CH (1976) Efficient estimation of free energy differences from Monte Carlo data. *J Comput Phys* 22(2):245–268.
40. Bussi G, Donadio D, Parrinello M (2007) Canonical sampling through velocity rescaling. *J Chem Phys* 126(1):014101.
41. Berendsen HJC, Postma JPM, van Gunsteren WF, DiNola A, Haak JR (1984) Molecular dynamics with coupling to an external bath. *J Chem Phys* 81(8):3684–3690.
42. Hess B (2008) P-LINCS: A parallel linear constraint solver for molecular simulation. *J Chem Theory Comput* 4(1):116–122.
43. Essmann U, et al. (1995) A smooth particle mesh Ewald method. *J Chem Phys* 103(19): 8577–8593.
44. Yamada A, Takeuchi K, Hishiyama M (1988) Intracellular processing of mumps virus glycoproteins. *Virology* 165(1):268–273.

Supporting Information

Kubota et al. 10.1073/pnas.1608383113

SI Materials and Methods

Viruses. EGFP-expressing recombinant MuVs of the Hoshino strain and SBL-1 strain were recovered from the respective full-length cDNA plasmids using the support plasmids encoding the MuV nucleocapsid, phospho, and large proteins (31). The MuV Tokyo S-III-10 and Tokyo M-21 strains are progenies of clinical isolates obtained from nasopharyngeal secretions (23).

Construction of Expression Plasmids. The DNA fragments encoding the HN/H and F proteins were amplified by PCR from the template plasmids of the MuV Hoshino strain (GenBank accession no. AB470486), PIV5 W3A strain (GenBank accession no. AF052755), PIV2 Toshiba strain (GenBank accession number NC_003443), SeV Z strain (GenBank accession number M30202), and measles virus Edmonston tag B strain (GenBank accession number Z66517). The amplified DNA fragments were cloned into the expression plasmid pCA7 (15). The cleavage site II sequence (amino acid positions 131–136, KKRKRR) of the respiratory syncytial virus F protein was inserted into the SeV-F sequence at Arg116 by site-directed mutagenesis to generate the SeV-F protein cleaved by furin (32). The plasmids encoding MuV, PIV5, PIV2, and SeV mutant HN proteins with alanine substitution at Tyr369, Trp352, Tyr357, and Trp373, respectively, were generated by PCR-based mutagenesis. The plasmids encoding WT and mutant HN proteins were generated such that they contained the C-terminal HA-tag for MuV and PIV2 and the His_6-tag for PIV5 and SeV, respectively. The plasmid encoding MuV-HN without the tag was produced as well. The expression plasmid encoding the tag-free MuV-HN protein was used in the experiments shown in Fig. 4*A*, Fig. S5 *C* and *D*, and Fig. S6*B*, and the plasmids encoding tag-containing MuV-, PIV5-, PIV2-, and SeV-HN proteins were used in the assays shown in Fig. 5 *A* and *B* and Fig. S6*A*. For the structural analysis of MuV-HN and the binding assay using sialyl glycopolymers (Fig. S4), the DNA fragment encoding the head domain of MuV-HN (amino acid positions 106–582) was amplified by PCR from the full-length cDNA of the Hoshino strain and cloned into the expression vector pHLsec containing the N-terminal secretion signal sequence and the C-terminal His_6-tag sequence (15). For the glycan-binding assay (Fig. 3 and Fig. S3) and ITC experiments (Fig. 2*B*), MuV-HN (SBL-1 strain, amino acid positions 96–582) were cloned into the pHLsec vector. Measles virus H (Edmonston tag B strain, amino acid positions 149–617) was cloned into the pHLsec vector for the glycan-binding assay (Fig. 3).

Protein Expression and Purification. The expression plasmid encoding MuV-HN was transiently transfected into 80% confluent 293S GnTI(−) cells (12) using polyethyleneimine-MAX (Polysciences). At 6 d posttransfection, the supernatant containing the secreted MuV-HN was harvested and then centrifuged to eliminate cell components. MuV-HN was purified using an Ni^{2+}-NTA affinity column (COSMOGEL His-Accept; Nacalai Tesque) in the purification buffer (50 mM NaH_2PO_4, 150 mM NaCl, and 10 mM imidazole, pH 8.0), and then eluted with the elution buffer (50 mM NaH_2PO_4, 150 mM NaCl, and 500 mM imidazole, pH 8.0). The eluted protein was treated with 20 mM dimethylamine-borane complex (Sigma-Aldrich) and 40 mM formaldehyde at 4 °C overnight to methylate lysine residues. The reaction was quenched in the process of changing the buffer to 100 mM NaCl and 20 mM Tris·HCl pH 8.0 during gel filtration with a Superdex 200GL 10/300 column (GE Healthcare). MuV-HN was concentrated using Amicon Ultra centifugal filters (Merck Millipore) to ∼10 mg/mL for crystallization. Measles virus H protein was expressed and purified following the same procedures as for MuV-HN proteins.

Crystallization and Structure Determination. Crystals were grown by hanging-drop vapor diffusion at 20 °C in a drop containing 0.7 μL each of MuV-HN (9.7 mg/mL) and crystallization buffer [1.95 M ammonium sulfate, 3% (vol/vol) glycerol, and 0.1 M sodium acetate pH 5.0]. Cocrystals with SLs were grown with a fivefold higher molar concentration of 3′-SL or 6′-SL sodium salt (Tokyo Chemical Industry) against MuV-HN in the crystallization buffer. For the data collection, the crystals were cryocooled (by a nitrogen gas stream, 100 K) in the original crystallization buffer containing 25% (vol/vol) glycerol. The crystals of MuV-HN alone and MuV-HN in complex with 3′-SL diffracted to 2.24 Å and 2.18 Å, respectively.

All of the diffraction datasets were collected on beam line BL-1A (using a Pilatus3 S6M detector) or AR-NE3A (using a Pilatus 2M-F detector) at the Photon Factory, and were processed and scaled using autoPROC (Global Phasing) based on XDS (33). The MuV-HN head domain structure was solved by the molecular replacement with Phaser (34) using the Newcastle disease virus HN protein as a search model (PDB ID code 1E8V). Further model refinement procedures were carried out using Phenix (35). Interactive manual model building and correction were performed using Coot (36). The final structure was refined to an R_{work} value of 20.2% and an R_{free} value of 22.2%. In the Ramachandran plot, 94.4% of the refined structure is in favored regions and 5.0% is in allowed regions. The structure of MuV-HN in complex with 3′-SL was solved by molecular replacement using the MuV-HN head domain obtained in this study. The final structure was refined to an R_{work} value of 17.6% and an R_{free} value of 19.1%. In the Ramachandran plot, 95.3% of the refined structure is in favored regions and 4.5% is in allowed regions. Detailed data collection and crystallographic statistics are summarized in Table S1. Figures were produced using PyMOL (DeLano Scientific LLC; www.pymol.org).

Free Energy Calculation. The crystal structure of the ligand (3′-SL)-bound form of MuV-HN was used to generate the initial structure for the MD simulation. Because MuV-HN formed a dimer in the crystal structure, we performed the MD simulation in this form. The N and C termini of each protein chain were capped with an acetyl group and an *N*-methyl group, respectively. All of the histidine residues were protonated on the Nε2 atom, and seven disulfide bonds were formed. The structure was first optimized and then immersed in a 136-Å cubic water box. Sodium ions were added to neutralize the system. The LEaP module of AmberTools 12 (37) was used to generate the initial model. The Amber ff12SB (37) and GLYCAM06j (38) force fields and the TIP3 model were used for the protein, sugar chain, and water, respectively. The system was gradually heated to 300 K in a 200-ps MD run with position restraints on the nonhydrogen atoms of the protein. The force constants of the restraints were 10 kcal mol^{-1} $Å^{-2}$. The pressure was then adjusted to 1.0×10^5 Pa in an 800-ps MD run, during which the force constants of the restraints were gradually decreased to zero. Subsequently, an unrestrained MD simulation was performed for 100 ns. The system reached equilibrium within the simulation time.

The ligand-free form of MuV-HN and the sugar chain alone were also equilibrated in the aqueous solution. Here the structure of the ligand-free form of MuV-HN was generated by removing

the ligand from the ligand-bound form. The structure of the sugar chain alone was generated using the LEaP module. The simulation protocols were the same as that for the ligand-bound form of MuV-HN, except that a 50-Å cubic water box was used and the unrestrained MD simulation was performed for 10 ns for the system of the sugar chain alone. The final coordinates served as the initial coordinates of the MD simulation for the free energy calculation.

The contributions of the Glc-3 moiety of the receptor sugar chain and Y369 of MuV-HN to the free energy of binding were calculated using the free energy cycles shown in Fig. 2*B*. ΔG_1 and ΔG_2 were defined as the free energy difference between the trisaccharide (3′-SL) alone and the disaccharide (Sia-1–Gal-2) alone and that between the trisaccharide–MuV-HN complex and the disaccharide–MuV-HN complex, respectively. The contribution of the Glc-3 moiety was calculated by $\Delta\Delta G = \Delta G_1 - \Delta G_2$ (Fig. S2*A*). Similarly, ΔG_3 and ΔG_4 were defined as the free energy difference between the ligand-free forms of the WT and the Y369A mutant of MuV-HN and that between the ligand-bound forms of the WT and the Y369A mutant, respectively. The contribution of Y369 was calculated by $\Delta\Delta G = \Delta G_3 - \Delta G_4$ (Fig. S2*B*). Each free energy difference was calculated by the Bennett acceptance ratio (BAR) method (39), where a part of the structure was transformed from one to the other (trisaccharide to disaccharide or tyrosine to alanine) in a stepwise manner. The transformations occurred only in one monomer of the MuV-HN dimer. We considered 39 intermediate states in each transformation process. For each of the 41 states (the 39 intermediate states plus the initial and final states), a 1-ns MD simulation was performed sequentially, and the samples for the BAR method were taken from the last 500 ps of each simulation. In all of the MD simulations, the temperature and pressure were controlled by the velocity rescaling method (40) and the weak coupling method (41), respectively. The bond lengths involving hydrogen atoms were constrained with the LINCS algorithm (42) to allow the use of a large time step (2 fs). The electrostatic interactions were calculated with the particle mesh Ewald method (43). The MD simulation was performed with Gromacs 5.0.5 (30). The free energy values were calculated with the g_bar module of Gromacs.

ITC. The purified MuV-HN protein was dialyzed in Tris buffer (20 mM Tris·HCl pH 7.4 and 100 mM NaCl). The glycans (3′−SL; Tokyo Chemical Industry and 3′ sialylgalactose; OligoTech) were dissolved in the same buffer as the MuV-HN protein. The ITC experiments were performed with a MicroCal Auto-iTC200 (Malvern Instruments). First, 2 μL of the glycan solution (2 mM) was titrated into the sample cell containing 200 μL of the 20 μM MuV-HN protein solution. The titrations were performed at 25 °C, with a reference power of 5 μcal/s and a stirring speed of 1,000 rpm. To measure the background heat, the glycan solution was injected into the buffer. The area of each titration peak was plotted against the molar ratio of ligand to protein, and the binding constants (K_a) were obtained by fitting the plots with a 1:1 binding model using Origin 7 (OriginLab).

Glycan-Binding Assay. The purified MuV-HN proteins (WT and the mutant with the Y369A substitution) were prepared at a concentration of 1 μg/mL diluted in the binding buffer (Rexxam). The purified measles virus H protein, a negative control, was diluted with the binding buffer at a concentration of 100 μg/mL The modified version of the Bio-Rex glycan chip (Rexxam) shown in Fig. 3*B* and Fig. S3 and the glycoconjugate-spotted (19) Bio-Rex epoxy-coated glass slide (Rexxam) shown in Fig. 3*A* were used for the glycan-binding assay based on an evanescent-field fluorescence-assisted detection principle (22). The diluted proteins (70 μL each) were applied to the glass chambers and incubated at room temperature with gentle shaking for 60 min. After removal of the protein solution from the chambers, 70 μL of the anti-His_6 tag cy3-conjugated Ab (Rockland) in the binding buffer was applied at the concentration of 5 ng/mL, followed by incubation at room temperature with gentle shaking for 60 min. The fluorescence of the glass chambers was measured with a Bio-Rex Scan 200 scanner (Rexxam).

Binding Assay with Virions and the Purified MuV-HN Protein. UniversalBIND microplates (Corning) coated with the two distinctive sialyl glycopolymers on a poly-α-L-glutamic acid backbone (Neu5Acα2,3Galβ1,4GlcNAcβ-pAP or Neu5Acα2,6Galβ1,4GlcNAcβ-pAP) were used in the assay (24) shown in Fig. S4. The microplates were washed with PBS without potassium [PBS(−)] and then treated with 0.5% BSA in 0.05% Tween 20 in PBS(−) (PBST) for 1 h. Then viral particles or the purified MuV-HN protein were incubated with the sialyl glycopolymers on the plates for 120 min at 4 °C. After washing with PBST, the wells were fixed with 10% (vol/vol) formalin in PBST for 30 min. The wells were then washed again with PBST and incubated with the first Abs for 1 h at 37 °C. The first Abs used were anti–MuV-HN Abs (44) (a mixture of the mouse monoclonal Abs provided by Dr. Akio Yamada) or the rabbit anti-human influenza A, B virus polyclonal Ab (M149; Takara). The anti–His-tag Ab (Penta-His mouse monoclonal Ab; Qiagen) was used to detect the MuV-HN protein bound to the sialyl glycopolymers. After washing with PBST, the wells were incubated with peroxidase-labeled second Ab (MAX-PO; Nichirei Bioscience) for 45 min at 37 °C. The wells were washed with PBST and then incubated with 1× TMB ELISA substrate solution (eBioscience) for 10 min. The reaction was quenched by the addition of 0.5 M H_2SO_4. Absorbance was detected at 450 nm with a microplate reader (Bio-Rad).

Fusion Assay. For the overlay fusion assay (Fig. 4*A* and Fig. S5 *C*–*E*), culture media of HEK293, NCI-H358, and IMR-32 cells in a 12-well dish (Corning) were replaced with Opti-MEM serum-free medium (Gibco). The cells were then transfected with 1 μg of the expression plasmid encoding EGFP using Polyethylenimine MAX (Polysciences). The culture medium was returned to the respective maintenance medium supplemented with 10% (vol/vol) FBS 5 h later. At 24 h after transfection, the EGFP-transfected cells were treated with sialidases for 20 h or left untreated. The sialidase-treated/untreated cells were detached from the dish and overlaid onto different HEK293 cells that had been transfected with 0.4 μg of the expression plasmid encoding MuV-HN and 1.5 μg of the expression plasmid encoding the MuV-F protein. The expression plasmids encoding the H and F proteins of the measles virus were transfected following the same procedure as for those of MuV. The cell–cell fusion was evaluated under fluorescence microscopy at 0, 15, 30, and 60 or 90 min after overlay.

For another cell–cell fusion assay (Fig. 5 *A* and *B* and Fig. S6*B*), HEK293, Vero, NCI-H358, and IMR-32 cells were transfected with 0.4 μg of the expression plasmid encoding the WT or mutant HN protein of MuV, PIV5, PIV2, or SeV; 1.0 μg of the plasmid encoding the F protein of those viruses; and 0.5 μg of the plasmid encoding EGFP. The cell–cell fusion was evaluated under fluorescence microscopy at 24–72 h posttransfection.

Virus Entry. The EGFP-expressing recombinant MuV Hoshino strain was 10-fold serially diluted in 10% (vol/vol) FBS/DMEM, and HEK293 cells cultured in a 24-well dish (Corning) were infected with this strain for 60 min at 37 °C. After aspiration of residual viruses, the cells were washed with PBS(−), and the medium was replaced with the maintenance medium [10% (vol/vol) FBS/DMEM]. EGFP-expressing cells were counted under fluorescence microscopy at 24 h postinfection. Among the wells infected with serially diluted virus preparations, the wells containing 10–150 EGFP-expressing cells were selected for counting.

Sialidase Treatment. *A. ureafaciens* sialidase cloned from *A. ureafaciens* (Nacalai Tesque) was added to the culture medium at 20 mU/mL to remove both α2,3- and α2,6-linked sialic acids on glycoproteins and glycolipids. Then α2,3-sialidase cloned from *S. typhimurium* LT2 (Takara Bio) was added to the culture medium at 200 mU/mL to remove α2,3-linked sialic acid on glycoproteins and glycolipids.

Flow Cytometry. To examine the expression of sialic acids (Fig. S5*A*), HEK293, NCI-H358, and IMR-32 cells pretreated or untreated with sialidases were washed with PBS(−) and then detached from the dish with 2 mM EDTA/PBS(−). The cells were incubated with 1% BSA/PBS(−) for 30 min at room temperature and then divided into three aliquots. These aliquots were incubated with biotinylated MAL II (Vector Laboratories), which binds to α2,3-linked sialic acid; biotinylated SNA (Vector Laboratories), which binds to α2,6-linked sialic acid; or the lectin-free medium [1% BSA/PBS(−)] for 30 min at 4 °C with gentle shaking. The cells were washed with 1% BSA/PBS(−) and incubated with FITC-avidin (UltraAvidin Fluorescein; Leinco Technologies) in 1% BSA/PBS(−) for 30 min at 4 °C with gentle shaking. After washing with 1% BSA/PBS(−), the cells were analyzed on a FACSCalibur flow cytometer (BD Biosciences).

To examine the cell surface expression of the HN proteins (Fig. S6*A*), in a 12-well dish (Corning), HEK293 cells or Vero cells were transfected with 1 μg each of the expression plasmids encoding the WT or mutant HN proteins or the empty vector, using Lipofectamine LTX with PLUS reagent (Invitrogen). At 48 h after transfection, the cells were washed with PBS(−) and then detached from the dish with 2 mM EDTA/PBS(−). The cells were incubated with the first Abs [Y-11: anti–HA-tag Ab (Santa Cruz Biotechnology) or anti–His-tag polyclonal Ab (MBL International), depending on the tags] in 1% FBS/PBS(−) for 90 min at 4 °C. After washing, the cells were incubated with the second Ab (anti-rabbit IgG FITC conjugate; Sigma-Aldrich) in 1% FBS/PBS(−) for 45 min at 4 °C. After washing with PBS(−), the cells were analyzed on a FACSCalibur flow cytometer.

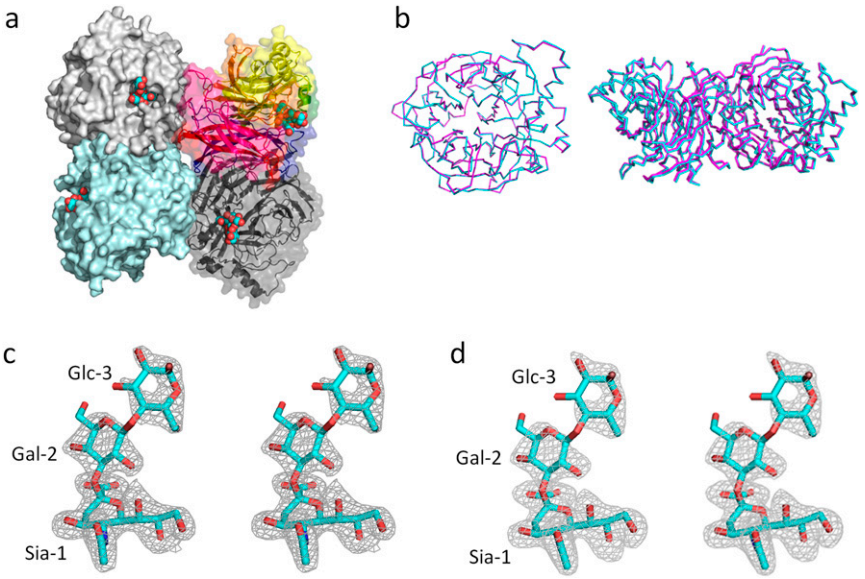

Fig. S1. Structures of MuV-HNs and 3′-SL. (*A*) Top view of the MuV-HN tetramer (dimer of dimers). Homodimer at upper left and lower left, surface diagram (light gray and pale cyan); another homodimer at upper right and lower right, ribbon and surface diagram (rainbow and dark gray) 3′-SLs, spheres. (*B*) MuV-HN monomer (*Left*, top view) and dimer (*Right*, side view) in which the form (cyan) obtained in the absence of receptor is superimposed on the 3′-SL–bound form (magenta). (*C* and *D*) Stereo views of the 2*Fo-Fc* map (1.5σ) (*C*) and omit *Fo-Fc* map (3.0σ) (*D*) of 3′-SL bound to MuV-HN. Color-coding is the same as in Fig. 1.

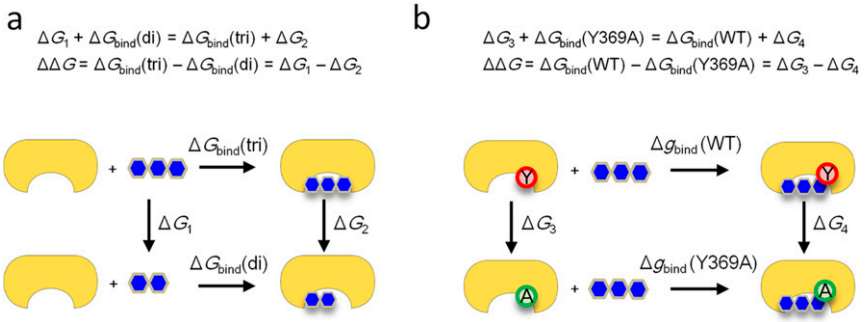

Fig. S2. Thermodynamic cycles used in the calculation of the free-energy changes. (*A*) The trisaccharide (3′-SL) was transformed into the disaccharide (Sai-1–Gal-2) in solution and in complex with the protein to calculate the free energy differences, ΔG_1 and ΔG_2, respectively. ΔG_{bind}(di) and ΔG_{bind}(tri) are the free energy changes on binding of the disaccharide and the trisaccharide to the protein, respectively. (*B*) Tyr369 of the protein was transformed into Ala in the ligand-free and ligand-bound states to calculate the free energy differences, ΔG_3 and ΔG_4, respectively. ΔG_{bind}(WT) and ΔG_{bind}(Y369A) are the free energy changes on binding of the trisaccharide to the WT and mutant proteins, respectively.

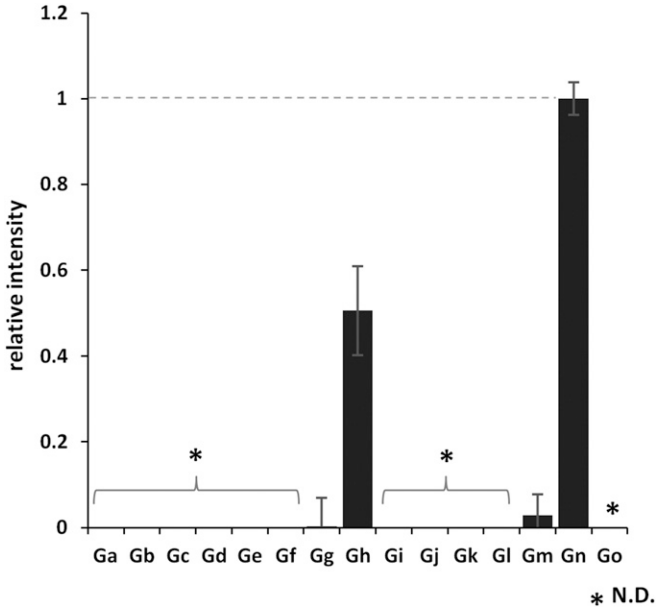

Fig. S3. Binding of the MuV-HN protein to 15 different glycans. All of the glycans are attached onto BSA except Gn and Go, which are conjugated with poly Glu. Ga, α-Man; Gb, α-Gal; Gc, β-Gal; Gd, α-GalNAc; Ge, β-GlcNAc; Gf, Galβ1,4Glc; Gg, Galβ1,4GlcNAc; Gh, NeuAcα2,3Galβ1,4Glc; Gi, NeuAcα2,6Galβ1,4Glc; Gj, Galβ1,3GalNac(T); Gk, Galβ1,3(GlcNAcβ1,6)GalNAc(Core2); Gl, Galβ1,3(Fucα1,4)GlcNAc(Le^a); Gm, Galβ1,4(Fucα1,3)GlcNAc(Le^x); Gn, NeuAcα2,3Galβ1,4GlcNAc-poly glutamic acid; Go, NeuAcα2,6Galβ1,4GlcNAc-poly glutamic acid. Data are mean ± SD of three samples. N.D., not detected. Data shown in this figure are representative of three independently performed experiments.

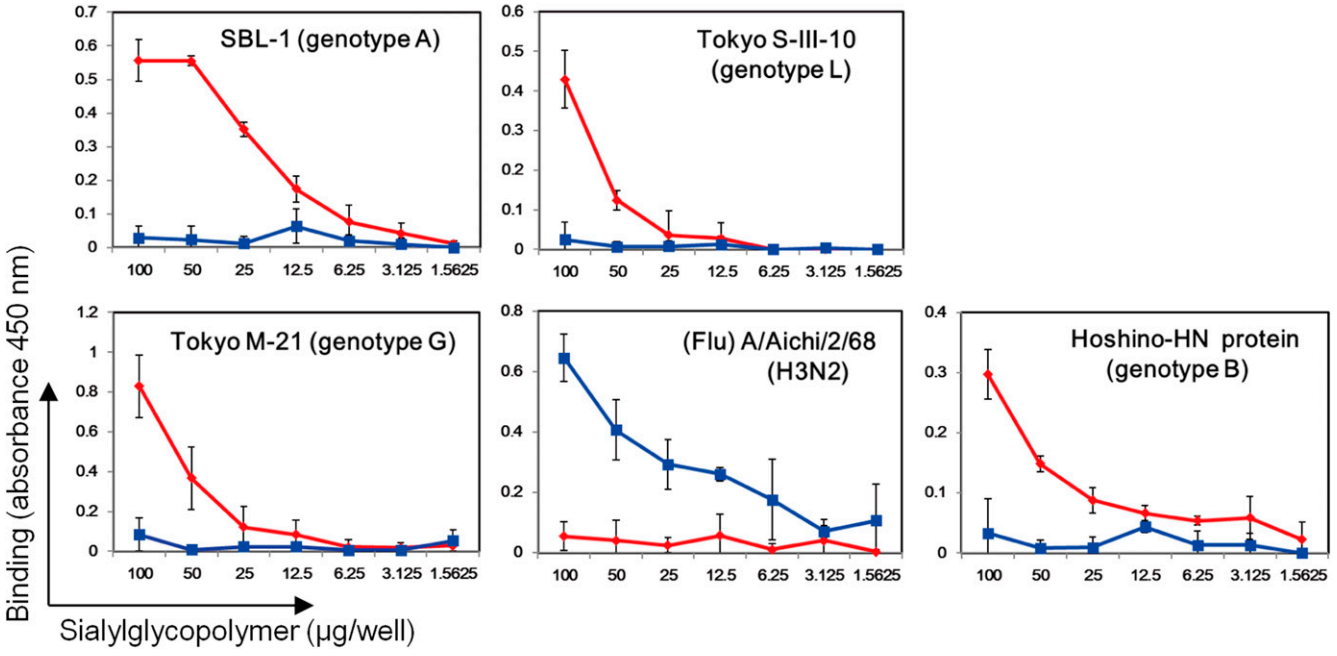

Fig. S4. Binding of MuVs to α2,3- and α2,6-linked sialyl glycopolymers. The mumps virions of the SBL-1, Tokyo S-III-10, and Tokyo M21 strains, along with the purified MuV-HN protein of the Hoshino strain containing the C-terminal His_6-tag sequence, were added to the microplates coated with serially diluted concentrations of α2,3- and α2,6-linked sialyl glycopolymers. Influenza virus (Flu) A/Aichi/2/68 (H3N2) served as a control. Bound virions and proteins were detected with anti–MuV-HN, anti–His-tag monoclonal Ab, or anti-influenza virus polyclonal Ab, followed by peroxidase-labeled secondary Ab. Absorbance at 450 nm is shown. Data are the mean ± SD of three samples. α2,3-linked sialyl glycopolymers are shown in red; α2,6-linked sialyl glycopolymers, in blue. The data are representative of three independently performed experiments.

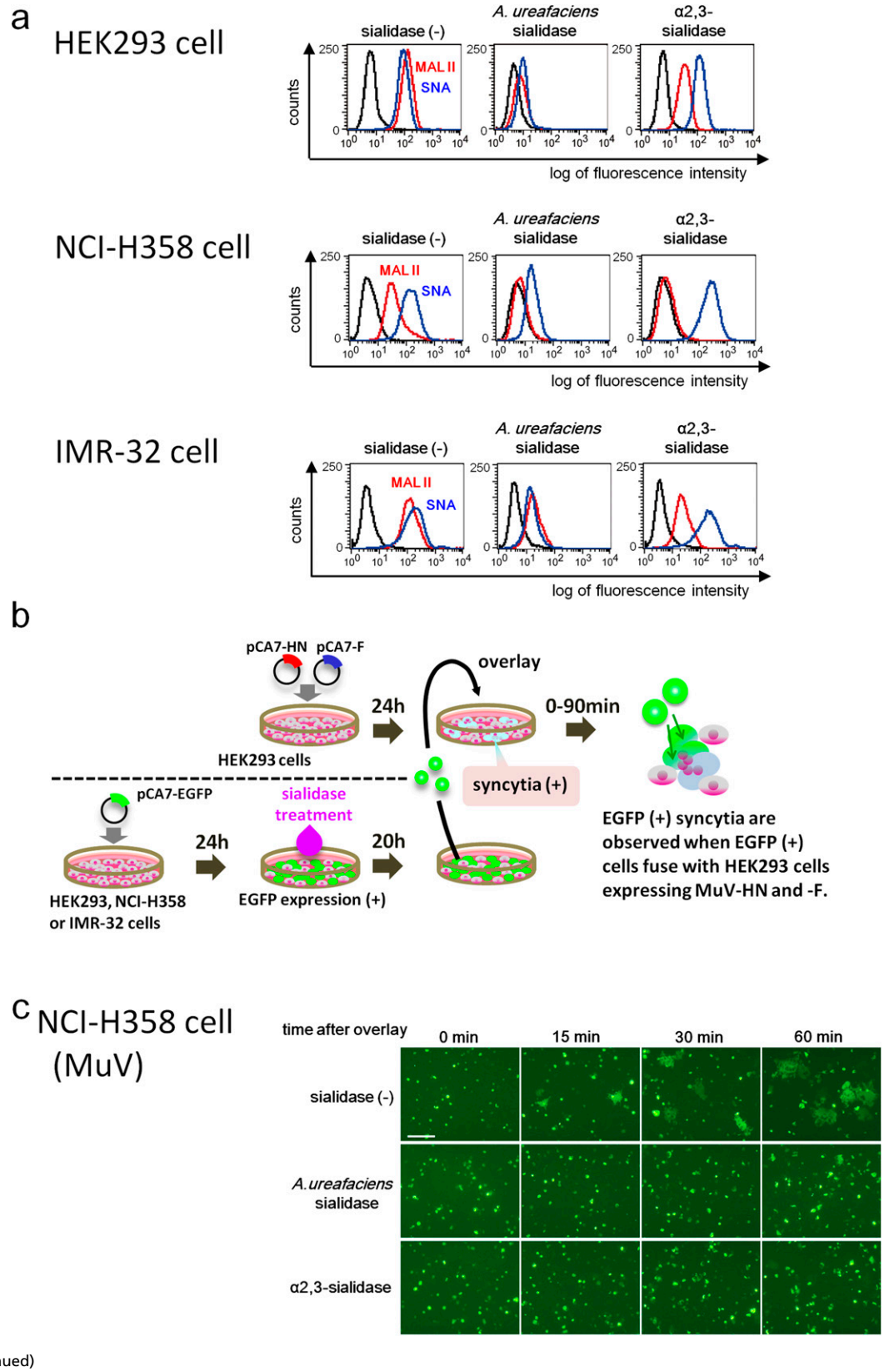

Fig. S5. (Continued)

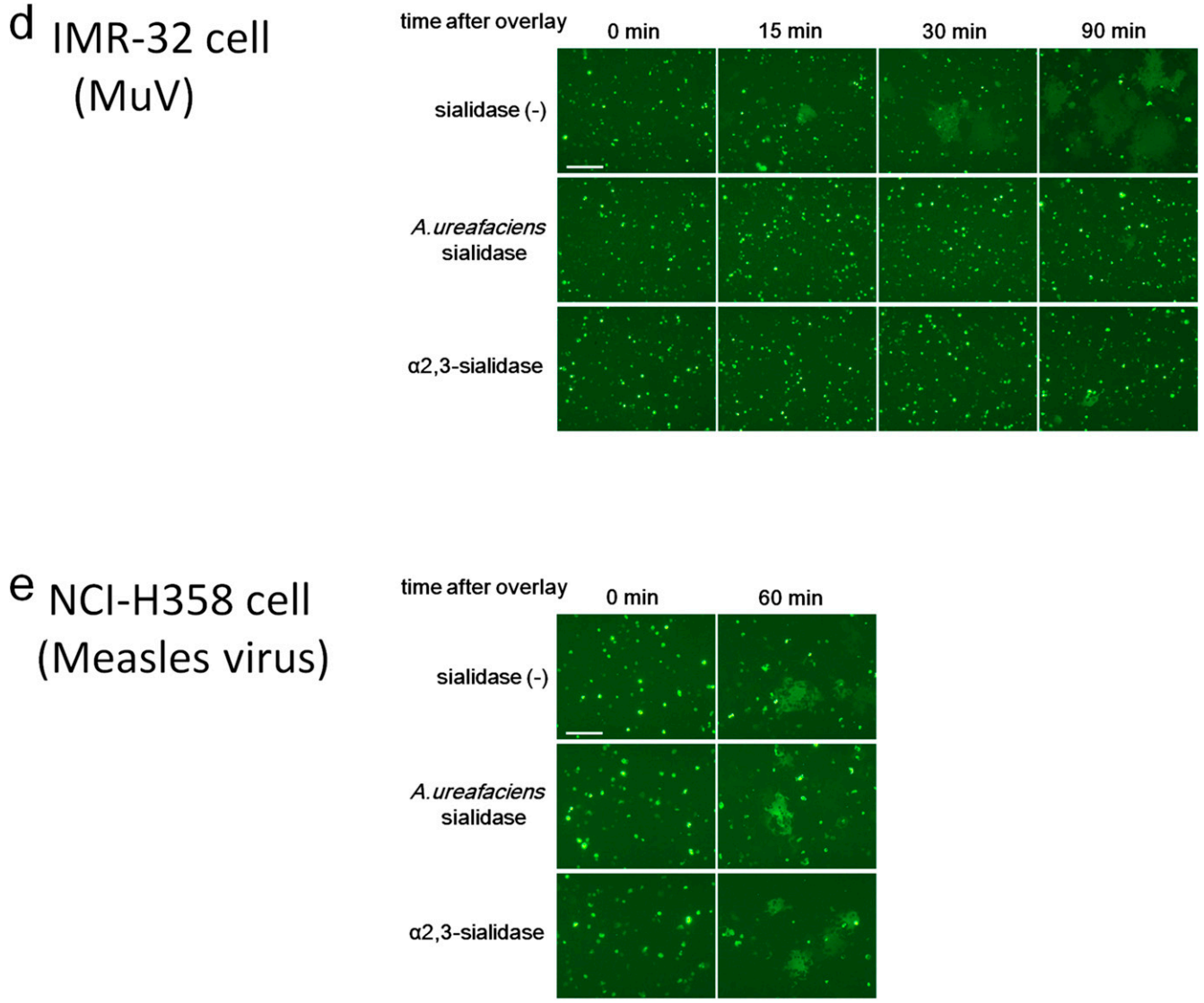

Fig. S5. Effect of cleavage of sialic acid on MuV-induced cell–cell fusion. (*A*) HEK293 cells, the respiratory epithelial cell line NCI-H358, and the neuroblastoma cell line IMR-32 were treated with control medium, *A. ureafaciens* sialidase, or *S. typhimurium* α2,3-sialidase. The treated cells were incubated with biotinylated MAL II, SNA, or control medium and then with FITC-avidin. They were analyzed on a FACSCalibur cell analyzer (BD Biosciences). (*B*) Schematic of the experimental procedure of the cell–cell fusion assay. (*C* and *D*) NCI-H358 cells (*C*) and IMR-32 cells (*D*) expressing EGFP were treated with control medium, α2,3-sialidase, or *A. ureafaciens* sialidase. They were detached from the plates and then overlaid onto HEK293 cells expressing the HN and F proteins of MuV. The cells were observed using fluorescent microscopy for up to 60 or 90 min after overlay. (*E*) Measles virus-induced cell–cell fusion was examined as a control. Sialidase-treated NCI-H358 cells were overlaid onto HEK293 cells expressing the H and F proteins of measles virus, and observed at 0 min and 60 min after overlay. (Scale bar: 200 μm.) The data are representative of three independently performed experiments.

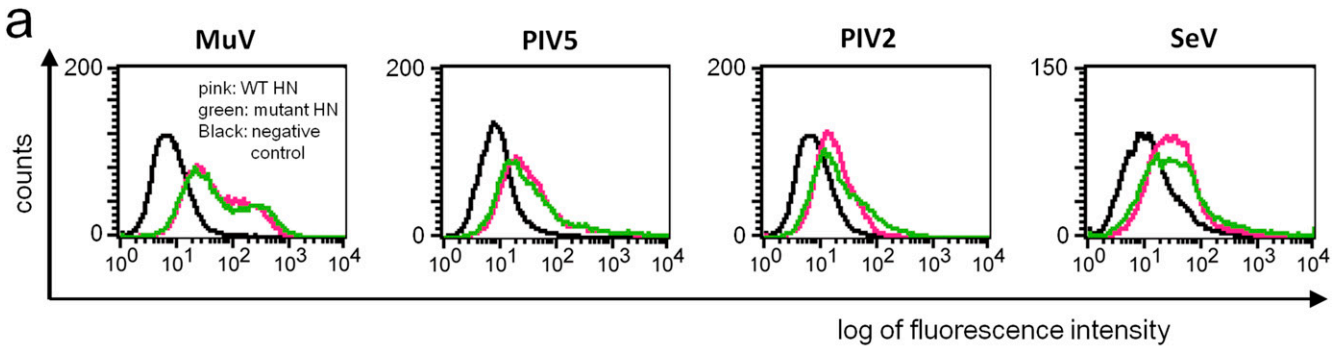

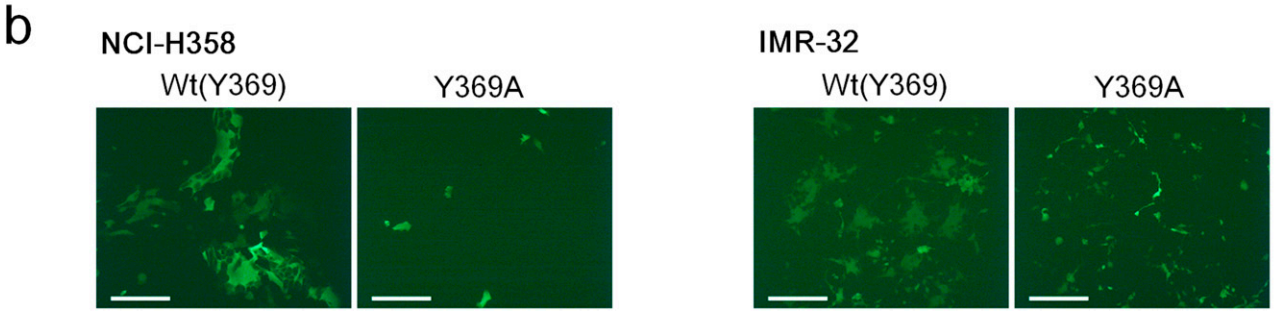

Fig. S6. Cell surface expression and fusion-supporting ability of WT and mutant HN proteins. (*A*) Expression of WT (pink) and mutant (green) HN proteins on transfected HEK293 (MuV, PIV5, and PIV2) or Vero (SeV) cells was examined by flow cytometry. Mutants have an alanine substituted for the residue interacting with the third sugar from the nonreducing terminal. The empty plasmid served as the control (black). (*B*) NCI-H358 and IMR-32 cells transfected with expression plasmids encoding the MuV-HN protein (WT or Y369A), MuV-F protein, and EGFP were observed for syncytia formation using fluorescent microscopy at 1 or 2 d after transfection. (Scale bar: 200 μm.) The data are representative of three independently performed experiments.

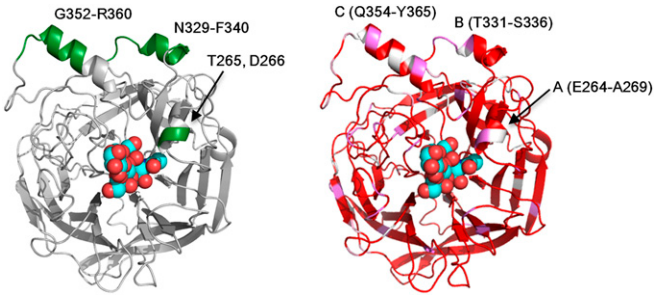

Fig. S7. Epitopes of neutralizing Abs against MuV-HN. (*Left*) Reported epitopes of neutralizing monoclonal Abs mapped on the structure of MuV-HN monomer (green). 3′-SL is shown in spheres. (*Right*) Sequence similarity of the HN proteins among the MuV reference strains from 12 genotypes mapped on the structure of MuV-HN monomer in gradation from red (identical), violet (strongly similar), and light pink (weakly similar) to white (different). A, B, and C are α-helices.

Table S1. Data collection and refinement statistics (molecular replacement)

Crystallographic parameters	Native MuV-HN	Native MuV-HN–3′-SL
Data collection		
Space group	$P6_1$	$P6_1$
Cell dimensions		
a, *b*, *c*, Å	137.52, 137.52, 178.27	136.88, 136.88, 177.27
α, β, γ, °	90.00, 90.00, 120.00	90.00, 90.00, 120.00
Resolution, Å	119.10–2.24 (2.245–2.238)	118.54–2.18 (2.184–2.177)
No. of reflections (observations)	937,606	979,751
No. of reflections (unique)	91,923	98,249
R_{sym}	0.159 (>1.00)	0.168 (>1.00)
R_{pim}	0.052 (0.556)	0.056 (0.398)
$I/\sigma I$	14.3 (2.1)	10.9 (2.0)
Completeness, %	100.0 (99.9)	100.0 (99.5)
Redundancy	10.2 (10.4)	10.0 (8.3)
CC (1/2)	0.997 (0.588)	0.994 (0.693)
Refinement		
Resolution, Å	119.10–2.24	118.54–2.18
No. of reflections	91,851	98,172
R_{work}/R_{free}	20.2/22.2	17.6/19.1
No. of atoms		
Protein	7,036	7,036
Ligand/ion	122	231
Water	174	234
B factors		
Protein	39.1	31.4
Ligand/ion	57.2	47.8
Water	34.6	30.2
rmsd		
Bond lengths, Å	0.004	0.006
Bond angles, °	0.888	1.109

Single-crystal X-ray diffraction data were collected for each structure. Values in parentheses are for highest resolution shell.